University Library



A gateway to Melbourne's research publications

Minerva Access is the Institutional Repository of The University of Melbourne

Author/s:
Kim, HS;Wyithe, JSB;Power, C;Park, J;Lagos, CDP;Baugh, CM

Title:
The HI mass function as a probe of photoionization feedback on low-mass galaxy formation

Date:
2015-11-01

Citation:
Kim, H. S., Wyithe, J. S. B., Power, C., Park, J., Lagos, C. D. P. & Baugh, C. M. (2015). The HI mass function as a probe of photoionization feedback on low-mass galaxy formation. Monthly Notices of the Royal Astronomical Society, 453 (3), pp.2315-2325. https://doi.org/10.1093/mnras/stv1822.

Persistent Link:
https://hdl.handle.net/11343/116524

Monthly Notices
of the
ROYAL ASTRONOMICAL SOCIETY

MNRAS **453,** 2315–2325 (2015) doi:10.1093/mnras/stv1822

The H I mass function as a probe of photoionization feedback on low-mass galaxy formation

Han-Seek Kim,[1⋆] J. S. B. Wyithe,[1,2] C. Power,[2,3] Jaehong Park,[1] C. d. P. Lagos[3] and C. M. Baugh[4]

[1]*School of Physics, The University of Melbourne, Parkville, VIC 3010, Australia*
[2]*ARC Centre of Excellence for All-sky Astrophysics (CAASTRO), 44 Rosehill Street Redfern, NSW 2016, Australia*
[3]*International Centre for Radio Astronomy Research, University of Western Australia, 35 Stirling Highway, Crawley, WA 6009, Australia*
[4]*Institute for Computational Cosmology, Department of Physics, University of Durham, South Road, Durham DH1 3LE, UK*

Accepted 2015 August 4. Received 2015 July 30; in original form 2015 June 5

ABSTRACT

We explore the galaxy formation physics governing the low-mass end of the H I mass function in the local Universe. Specifically, we predict the effects on the H I mass function of varying (i) the strength of photoionization feedback and the redshift of the end of the epoch of reionization, (ii) the cosmology, (iii) the supernovae feedback prescription and (iv) the efficiency of star formation. We find that the shape of the low-mass end of the H I mass function is most affected by the critical halo mass below which galaxy formation is suppressed by photoionization heating of the intergalactic medium. We model the redshift dependence of this critical dark matter halo mass by requiring a match to the low-mass end of the H I mass function. The best-fitting critical dark matter halo mass decreases as redshift increases in this model, corresponding to a circular velocity of $\sim$50 km s^{-1} at $z = 0$, $\sim$30 km s^{-1} at $z \sim 1$ and $\sim$12 km s^{-1} at $z = 6$. We find that an evolving critical halo mass is required to explain both the shape and abundance of galaxies in the H I mass function below $M_{\rm H\,I} \sim 10^8\,h^{-2}\,{\rm M}_\odot$. The model makes specific predictions for the clustering strength of H I-selected galaxies with H I masses $>10^6$ and $>10^7\,h^{-2}\,{\rm M}_\odot$ and for the relation between the H I and stellar mass contents of galaxies which will be testable with upcoming surveys with the Square Kilometre Array and its pathfinders. We conclude that measurements of the H I mass function at $z \geq 0$ will lead to an improvement in our understanding of the net effect of photoionization feedback on galaxy formation and evolution.

Key words: galaxies: evolution – galaxies: formation – large-scale structure of Universe – radio lines: galaxies.

1 INTRODUCTION

There is a wealth of observational evidence that the Universe experienced an 'epoch of reionization' (EoR) at $z \geq 6$ (e.g. Ouchi et al. 2010; Mesinger, Furlanetto & Cen 2011; McGreer, Mesinger & Fan 2011; Shull et al. 2012) during which time the cosmic diffuse neutral hydrogen was 'reionized' by a background of ultraviolet (UV) and X-ray radiation produced by the first generation of stars and galaxies (e.g. Barkana & Loeb 2007; Robertson et al. 2010). This photoionizing background heated the gas in low-mass dark matter haloes, leading to its expulsion from their shallow potential wells (Shapiro, Iliev & Raga 2004). In addition, an increased Jeans mass prevented infall of gas on to low-mass haloes with virial temperatures $\leq 10^4$ K (cf. Efstathiou 1992). This implies that there should be a critical dark matter halo mass – and therefore a halo circular velocity – below which galaxy formation should be suppressed during reionization. Recently, Brown et al. (2014) presented high-resolution spectroscopy of stars in six ultra-faint dwarfs within the vicinity of the Milky Way and analysed their stellar population properties. Brown et al. concluded that these galaxies formed $\sim$80 per cent of their stars by $z \sim 6$, and therefore are the best nearby candidates for probing star formation (SF) quenching during the EoR. These galaxies have maximum velocities $\sim$10 km s^{-1}, imposing an observational limit for SF quenching due to the reionization.

Rees (1986) used analytical arguments to deduce that this critical circular velocity should be $V_{\rm cut} \simeq 30\,{\rm km\,s^{-1}}$, reasoning that the rate at which gas is heated by an ionizing background is balanced by the rate at which it cools radiatively. Subsequent studies have tried to sharpen the prediction for $V_{\rm cut}$, with calculations based

⋆E-mail: hansikk@unimelb.edu.au

© 2015 The Authors
Published by Oxford University Press on behalf of the Royal Astronomical Society

Downloaded from http://mnras.oxfordjournals.org/ at University of Melbourne on February 15, 2016

on semi-analytic approaches (e.g. Efstathiou 1992; Benson et al. 2002), idealized 1D hydrodynamical calculations (e.g. Thoul & Weinberg 1996) and fully cosmological hydrodynamical simulations (e.g. Gnedin 2000; Okamoto, Gao & Theuns 2008). However, there is still debate about the precise value of $V_{\rm cut}$. Recently, Sobacchi & Mesinger (2013, hereafter SM2013) used 1D collapse simulations to show that the critical halo mass depends on the redshift, following earlier work by Dijkstra et al. (2004).

The H I mass function in the local Universe provides information about galaxy formation physics in low-mass dark matter haloes. Indeed, Kim et al. (2013a) recently showed that feedback effects are important in determining the H I mass function in the local Universe. In particular, the low-mass end of the H I mass function is governed by photoionization feedback processes in small dark matter haloes. In this paper, we discuss the question of whether such modelling can be used to gain further insight into the value of $V_{\rm cut}$. Specifically, we explore the effect of photoionization feedback on the H I mass function using the GALFORM semi-analytic galaxy formation model Cole et al. (2000). This model reproduces the observed H I mass function at $z = 0$, accurately matching its amplitude and shape at intermediate and high H I masses. We compare the models with observational estimates of the H I mass function from the H I Parkes All-Sky Survey (HIPASS; see Meyer et al. 2004) and Arecibo Legacy Fast ALFA Survey (ALFALFA; see Giovanelli et al. 2005) surveys. We use the version of the semi-analytical galaxy formation model GALFORM developed by Lagos et al. (2011a, 2012) as the default model.

The structure of the paper is as follows. In Section 2, we provide a brief overview of the Lagos et al. (2011a) model. In Section 3, we show how the different ingredients influence the H I mass function. In Section 4, we describe the modified model for photoionization feedback. We finish with a summary of our results in Section 6.

2 THE GALAXY FORMATION MODEL

We use the semi-analytical galaxy formation model GALFORM (cf. Cole et al. 2000; Baugh 2006) described in Lagos et al. (2011a, 2012) to predict the properties of galaxies forming and evolving in the Λ cold dark matter (ΛCDM) cosmology.[1] GALFORM models the key physical processes of galaxy formation, including the gravitationally driven assembly of dark matter haloes, radiative cooling of gas and its collapse to form centrifugally supported discs, SF, and feedback from supernovae (SNe) and active galactic nuclei (AGNs).

Lagos et al. (2011a) extended GALFORM by modelling the splitting of cold gas in the interstellar medium into its H I and H_2 components and by explicitly linking SF to the amount of H_2 present in a galaxy. Lagos et al. (2011a) compared empirically and theoretically derived SF laws (cf. Blitz & Rosolowsky 2006; Krumholz, McKee & Tumlinson 2009) with a variety of observations [e.g. the H I mass function, ^{12}CO (1–0) luminosity function, and correlations between the ratio H_2/H I and stellar and cold gas masses in Lagos et al. (2012)] and found that the empirical law of Blitz & Rosolowsky (2006, see also Leroy et al. 2008) is favoured by these data. This law is of the form

$$\Sigma_{\rm SFR} = \nu_{\rm SF}\, f_{\rm mol}\, \Sigma_{\rm gas}, \qquad (1)$$

where $\Sigma_{\rm SFR}$ and $\Sigma_{\rm gas}$ are the surface densities of the star formation rate (SFR) and total cold gas mass, respectively, $\nu_{\rm SF}$ is the inverse of the SF time-scale for the molecular gas and $f_{\rm mol} = \Sigma_{\rm mol}/\Sigma_{\rm gas} = R_{\rm mol}/(R_{\rm mol}+1)$ is the molecular to total gas mass surface density ratio. $R_{\rm mol}$ is defined by $R_{\rm mol} = \Sigma({\rm H_2})/\Sigma({\rm H\,I}) = (P_{\rm ext}/P_0)^{\beta_{\rm press}}$. $P_{\rm ext}$ is the interstellar gas pressure in a galaxy. We calculate $P_{\rm ext}$ using the approximation from Elmegreen (1993),

$$P_{\rm ext} \approx \frac{\pi}{2} G\, \Sigma_{\rm gas} \left[\Sigma_{\rm gas} + \left(\frac{\sigma_g}{\sigma_*}\right) \Sigma_*\right], \qquad (2)$$

where G is the gravitational constant and Σ_* is the total surface densities of the stars. The velocities dispersions of the gas and stars are given, respectively, by $\sigma_{\rm gas}$ and σ_*. The values allowed by the observations of Leroy et al. (2008) and Bigiel et al. (2010) are $\nu_{\rm SF} = 0.52 \pm 0.25\,{\rm Gyr^{-1}}$, $\log(P_0/k_{\rm B}({\rm cm^{-3}\,K})) = 4.54 \pm 0.07$ and $\beta_{\rm press} = 0.92 \pm 0.07$. Importantly for the work we present in this paper, Lagos et al. (2011b) showed that the Blitz & Rosolowsky (2006) law is able to broadly reproduce the H I mass function at $z = 0$ at high and intermediate H I masses, $M_{\rm H\,I} > 10^8\,h^{-2}\,{\rm M_\odot}$. This is because it suppresses SF in lower mass galaxies due to their low $\Sigma_{\rm gas}$, thereby reducing SNe feedback and allowing these galaxies to retain larger gas reservoirs. Note that we use the Lagos et al. (2012) model as the default model in this paper. In addition to the Blitz & Rosolowsky (2006) SF law, this model has longer duration starbursts compared with the model of Bower et al. (2006).

As discussed in Kim et al. (2013a), photoionization is predicted to have a dramatic impact on SF in low-mass galaxies. This is because the presence of a photoionizing background both modifies the net cooling rate of gas in haloes by removing the 'hydrogen peak' in the cooling curve (cf. fig. 1 of Benson et al. 2002) and increases the temperature of the intergalactic medium such that its thermal pressure prevents gravitational collapse on to low-mass haloes (e.g. Efstathiou 1992; Okamoto et al. 2008). As a result, only those haloes that hosted cold gas prior to reionization can form stars (e.g. Hoeft et al. 2006). GALFORM includes the Benson et al. (2002) prescription for suppressing the cooling of halo gas on to the galaxy – this occurs if the host halo's circular velocity $V_{\rm circ}$ lies below a threshold $V_{\rm cut}$ at redshift $z_{\rm cut}$. The values in the default Lagos et al. (2012) model are $V_{\rm cut} = 30\,{\rm km\,s^{-1}}$ and $z_{\rm cut} = 10$. The default $V_{\rm cut}$ is motivated by the results of hydrodynamical simulations by Hoeft et al. (2006) and Okamoto et al. (2008). However, several studies indicate that $V_{\rm cut}$ should be redshift dependent (Dijkstra et al. 2004; Sobacchi & Mesinger 2013). The implementation of a single value of $z_{\rm cut}$ and $V_{\rm cut}$ may therefore be overly simplistic. We revise this modelling in this paper.

3 UNDERSTANDING THE LOW-MASS END OF H I MASS FUNCTION IN THE LOCAL UNIVERSE

The self-consistent treatment of H I in Lagos et al. (2011a, 2012) results in a model that shows good agreement between model predictions and the HIPASS and ALFALFA observations for H I masses greater than $M_{\rm H\,I} \sim 10^8\,h^{-2}\,{\rm M_\odot}$. However, the predicted H I mass function between 10^6 and $10^8\,h^{-2}\,{\rm M_\odot}$ (i.e. the low-mass end of the H I mass function) fails to capture the shape and abundance of the observed H I mass function. In this section, we investigate how predictions of the low-mass end of the H I mass function at $z \simeq 0$ are influenced by the assumed photoionizing background feedback, cosmology, SNe feedback prescription and SF law efficiency. We also introduce a description of the possible redshift dependence of the photoionizing feedback strength. Throughout

[1] Recall that the cosmological parameters adopted for the Millennium Simulation are the total matter density $\Omega_{\rm M} = 0.25$, the baryon density $\Omega_{\rm b} = 0.045$, the vacuum energy density $\Omega_\Lambda = 0.75$, the Hubble parameter $H_0 = 73\,{\rm km\,s^{-1}\,Mpc^{-1}}$, the primordial scalar spectral index $n_{\rm s} = 1$ and the fluctuation amplitude $\sigma_8 = 0.9$.

Downloaded from http://mnras.oxfordjournals.org/ at University of Melbourne on February 15, 2016

the paper, we use Monte Carlo generated merger histories (Parkinson, Cole & Helly 2008). We adopt a minimum halo mass of $M_{\rm halo,\,min} = 5 \times 10^8\,h^{-1}\,{\rm M}_\odot$. From the chosen minimum halo mass, we can predict the neutral hydrogen gas mass structures down to the current observational limits (Martin et al. 2010).

3.1 Photoionization feedback at the end of reionization

In the standard implementation of GALFORM, the effect of photoionization feedback induced by the EoR is modelled by imposing a circular velocity cut-off $V_{\rm cut}$ on galaxy formation at a redshift of the end of reionization $z_{\rm cut}$. In Fig. 1, we show the resulting H I mass function assuming this standard model for reionization for a range of photoionization strengths $V_{\rm cut}$ (at fixed $z_{\rm cut}$) and redshifts marking the end of reionizaiton $z_{\rm cut}$ (at fixed $V_{\rm cut} = 30\,{\rm km\,s^{-1}}$). These models can be compared with observations from ALFALFA (Martin et al. 2010) and HIPASS (Zwaan et al. 2005). The single values of $V_{\rm cut}$ and $z_{\rm cut}$ introduce a non-monotonic feature in the H I mass function that is not present in the observations. The top panel of Fig. 1 shows that the predicted abundance of galaxies with $2\times10^7\,h^{-2}\,{\rm M}_\odot < M_{\rm H\,I} < 10^8\,h^{-2}\,{\rm M}_\odot$ is larger than observed when we choose the $V_{\rm cut} = 25\,{\rm km\,s^{-1}}$, which matches the abundance at $M_{\rm H\,I} < 10^7\,h^{-2}\,{\rm M}_\odot$ (red dotted line). In contrast, the predicted abundance of galaxies with $M_{\rm H\,I} < 10^7\,h^{-2}\,{\rm M}_\odot$ is lower than observed when we select $V_{\rm cut} = 35\,{\rm km\,s^{-1}}$, which fits the abundance of galaxies with $2 \times 10^7\,h^{-2}\,{\rm M}_\odot < M_{\rm H\,I} < 10^8\,h^{-2}\,{\rm M}_\odot$. This is evidence of the simple modelling of photoionization feedback leading to the non-monotonic feature discussed above.

We also investigate the effect of varying the redshift of reionization at a fixed $V_{\rm cut} = 30\,{\rm km\,s^{-1}}$. The bottom panel of Fig. 1 shows that the value of $z_{\rm cut}$ does not influence the low-mass end of the H I mass function for values ranging between $z_{\rm cut} = 1$ and 10 (in the case of $V_{\rm cut} = 30\,{\rm km\,s^{-1}}$) indicating that the H I mass function in the local Universe cannot be used as a probe of the end of the EoR, at least using this simple modelling of photoionization feedback.

3.2 Other possibilities: cosmology, supernova feedback recipe and star formation law

In this subsection, we explore the effects of a range of additional aspects of galaxy formation on the H I mass function.

First, we inspect the impact of cosmology (top panel of Fig. 2). The default model has the cosmology used in the Millennium *N*-body simulation of Springel et al. (2005) as noted in Section 2. This is compared with a model having the WMAP7 cosmology for which the parameters in GALFORM have been adjusted to reproduce a suite of other observations (Gonzalez-Perez et al. 2014). The abundance of galaxies across the full mass range of H I masses in the WMAP7 cosmology is larger than in the Millennium cosmology. However, the non-monotonic feature described in the last subsection remains and therefore is not dependent on cosmology.

Secondly, we have explored the SNe saturation model suggested by Font et al. (2011). The default GALFORM model parametrizes the SNe feedback mass loading efficiency as $\beta = (V_{\rm circ}/V_{\rm hot})^{-\alpha_{\rm hot}}$, where $V_{\rm circ}$ is the circular velocity of the galaxy at the half-mass radius. The parameters $V_{\rm hot}$ and $\alpha_{\rm hot}$ are adjustable and control the strength of SNe feedback. The default model has $V_{\rm hot} = 485\,{\rm km\,s^{-1}}$ and $\alpha_{\rm hot} = 3.2$ (cf. Bower et al. 2006). In order to fit the number of satellite galaxies and their metallicity in the Milky Way, Font et al. (2011) proposed a scenario in which the SNe feedback efficiency is not a simple power law for all galaxy masses (as it is in the default model). They modelled an efficiency of SNe feedback that saturates

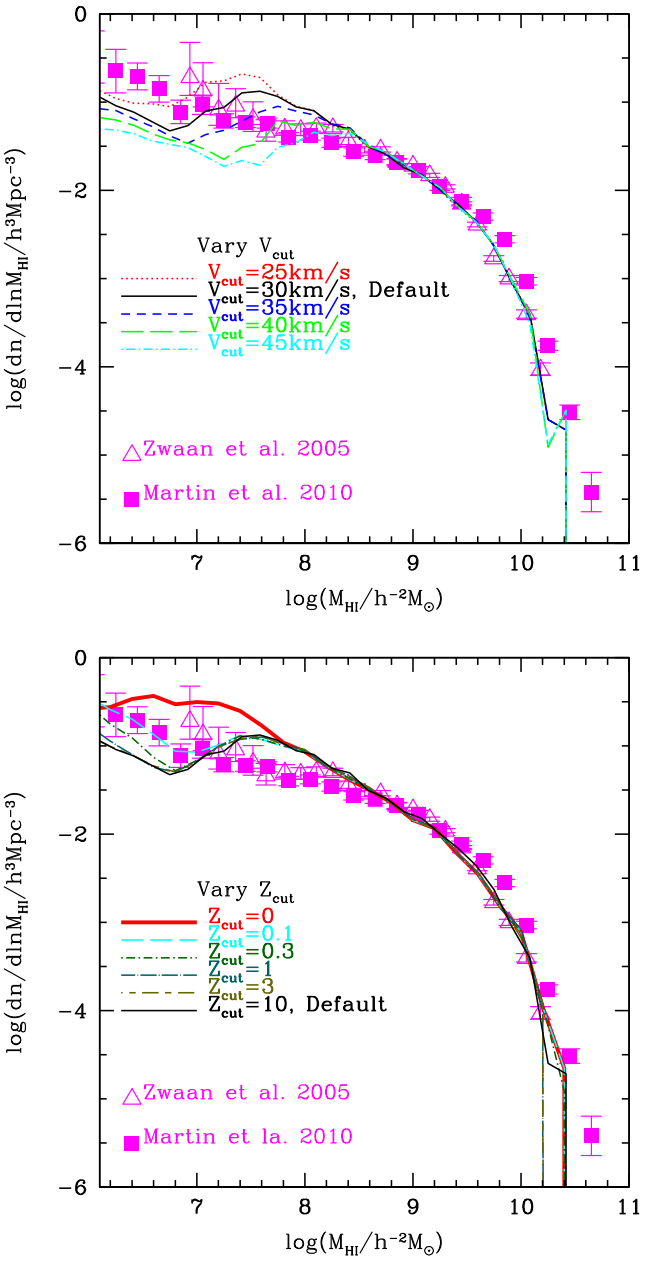


Figure 1. The impact of the photoionizing background on the predicted H I mass function. The panels show models for varying $V_{\rm cut}$ (top panel) and $z_{\rm cut}$ values (bottom panel). The symbols correspond to observations from HIPASS (open triangles; cf. Zwaan et al. 2005) and ALFALFA (filled squares; cf. Martin et al. 2010). We vary the photoionization strength between $25\,{\rm km\,s^{-1}} \le V_{\rm cut} \le 45\,{\rm km\,s^{-1}}$ (at a fixed $z_{\rm cut} = 10$) and $0 \le z_{\rm cut} \le 10$ (at a fixed $V_{\rm cut} = 30\,{\rm km\,s^{-1}}$), as labelled in each panel.

in low-mass galaxies with circular velocities less than $65\,{\rm km\,s^{-1}}$, but which follows the default model for larger galaxies (see Lagos, Lacey & Baugh 2013, for a physical interpretation of this saturation). Here, we define the circular velocity of saturated low-mass galaxies as $V_{\rm sat}$, and explore the impact on the H I mass function of varying $V_{\rm sat}$ (from 0 to $70\,{\rm km\,s^{-1}}$, middle panel of Fig. 2). The abundance of galaxies with $M_{\rm H\,I} < 10^7\,h^{-2}\,{\rm M}_\odot$ increases as the value of $V_{\rm sat}$ increases, because less gas is reheated and expelled from the disc to the halo when the galaxy has circular velocity $V_{\rm circ} \le V_{\rm sat}$. However, as we found for the case of changing cosmology, the

Downloaded from http://mnras.oxfordjournals.org/ at University of Melbourne on February 15, 2016

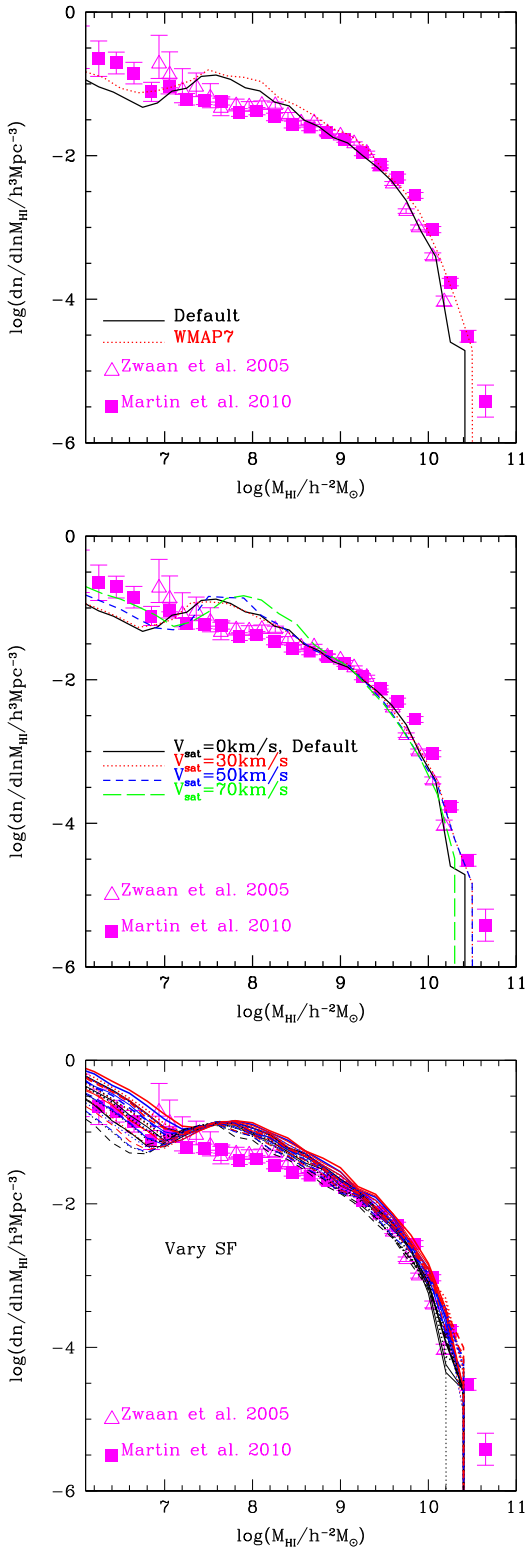


Figure 2. Impact of various galaxy formation physics on the H I mass function. Top panel: the effect of the changing the cosmology from WMAP1 to WMAP7. Middle panel: the effect of varying the circular velocity below which supernova feedback saturates, as described in Font et al. (2011). Bottom panel: the effect of varying the parameters in the star formation law from Lagos et al. (2012) within the observational constraints (see text for details). The symbols correspond to data from HIPASS (open triangles; cf. Zwaan et al. 2005) and ALFALFA (filled squares; cf. Martin et al. 2010).

non-monotonic feature is still present in the predicted H I mass function even after varying $V_{\rm sat}$.

In addition, we explore the effect of changing the parameters of the SF law within the observed range as noted in Section 2. The bottom panel of Fig. 2 shows the H I mass function resulting from varying values of $\nu_{\rm SF} = [0.27, 0.5, 0.755]$ (solid, dotted, dashed lines) Gyr^{-1}, $P_0/k_{\rm B} = [17000, 30000, 40738]$ (black, blue, red line) cm^{-3} K and $\beta_{\rm press} = [0.8, 0.9, 0.99]$ (the thinnest to the thickest). We show the H I mass functions from the sets of 27 combinations of three parameters of the SF law. The varied $\nu_{\rm SF}$ and P_0 values lead to an overall shift in the H I mass function compared to the default model. Varying the value of $\beta_{\rm press}$ also produces an overall shift in the mass function. In addition, varying $\beta_{\rm press}$ results in a large change in abundance at the low-mass end of the H I mass function. This change is most likely due to a lower $\Sigma_{\rm H2}/\Sigma_{\rm H\,I}$ in the regime $P_{\rm ext} < P_0$ (H I-dominated regions) which is obtained for large values of $\beta_{\rm press} \sim 0.99$.

However, as in the cases of varying cosmology and SNe feedback, changing the SF law still results in a non-monotonic H I mass function for $M_{\rm H\,I} \leq 10^8\,h^{-2}\,{\rm M}_\odot$ in all 27 cases, in disagreement with observations. This suggests that new or modified physics is needed in the default galaxy formation model in order to improve the agreement with the observations at $M_{\rm H\,I} \leq 10^8\,h^{-2}\,{\rm M}_\odot$.

4 AN IMPROVED MODEL FOR PHOTOIONIZATION FEEDBACK

In the previous section, we explored a range of possibilities for phenomena which may govern the low- and intermediate-mass range of the H I mass function. In all cases, the predictions include a non-monotonic feature which is not present in the observations. The results of Fig. 1 suggest that the non-monotonic feature in the low-mass end of the H I mass function is an artefact of adopting a single value of $V_{\rm cut}$ in the parametrization of photoionization feedback. We therefore model photoionization feedback using a redshift dependent $V_{\rm cut}(z)$ which is motivated by the calculations of Sobacchi & Mesinger (2013) using 1D collapse simulations. Note that in our default model, we use $\beta_{\rm press} = 0.99$ in the SF law.

Sobacchi & Mesinger (2013) assumed the following functional form for the critical mass, $M_{\rm crit}$, defined as the total halo mass where the baryon fraction is half of the global value:

$$M_{\rm crit} = M_0 J_{21}^a \left(\frac{1+z}{10}\right)^b \left[1 - \left(\frac{1+z}{1+z_{\rm IN}}\right)^c\right]^d, \quad (3)$$

where M_0, a, b, c and d are parameters that Sobacchi & Mesinger fitted to the results of their numerical simulations. The square bracketed term of equation (3) is related to the redshift evolution of the UVB exposure and redshift. The parameter $z_{\rm IN}$ corresponds to the redshift at which the halo was exposed to a UV background. Sobacchi & Mesinger (2013) explored a large parameter space of halo mass (M_0), UV background intensity (J_{21}, expressed in units of 10^{-21} erg s^{-1} Hz^{-1}cm^{-2} sr^{-1}), redshift (z) and redshift of UV background exposure ($z_{\rm IN}$) of galaxies. These are uncertain because the details of how reionization proceeded are yet to be observed.

Sobacchi & Mesinger (2013) quoted the best-fitting values of the parameters in equation (3) to their simulation results as (M_0, a, b, c, d) = ($2.8 \times 10^9\,{\rm M}_\odot$, 0.17, −2.1, 2.0, 2.5). For our purposes, it is helpful to recast the critical halo mass as a circular velocity, $V_{\rm cut}$ (Cole et al. 1994)

$$M_{\rm crit} = 3.36 \times 10^5 \left(\frac{V_{\rm cut}}{\rm km\,s^{-1}}\right)^3 (1+z)^{-\frac{3}{2}}\,{\rm M}_\odot, \quad (4)$$

Downloaded from http://mnras.oxfordjournals.org/ at University of Melbourne on February 15, 2016

where we have assumed a Hubble constant of $70\,\mathrm{km\,s^{-1}\,Mpc^{-1}}$. Combining equations (3) and (4), we obtain a redshift-dependent $V_{\rm cut}(z)$, which, after adopting the suggested best-fitting values for the parameters b, c and d for equation (3) is given by

$$V_{\rm cut}(z)(\mathrm{km\,s^{-1}}) = V_{\rm cut0}(1+z)^{\alpha_v}\left[1-\left(\frac{1+z}{1+z_{\rm IN}}\right)^2\right]^{2.5/3}. \quad (5)$$

Here the $V_{\rm cut0}$ is the circular velocity of dark matter haloes at $z = 0$ below which photoionization feedback suppresses gas cooling and $\alpha_v = b/3 + 1/2$ in the notation of Sobacchi & Mesinger. For the best-fitting value of $b = -2.1$, $\alpha_v = -0.2$. For simplicity, we assume the redshift of UV background exposure to be $z_{\rm IN} = 10$. The value of $V_{\rm cut0}$ is $\approx 100\,\mathrm{km\,s^{-1}}$ if we set $J_{21} = 1$. If we use this value of $V_{\rm cut0}$, the model underpredicts the low-mass end of the H I mass function by a substantial amount and also underpredicts the faint-end of the galaxy luminosity function in the optical. We find that the model gives a better match to the observed H I mass function if we instead use a critical mass at $z = 0$ which is reduced by a factor of 10 with respect to the value advocated by Sobacchi & Mesinger, corresponding to $V_{\rm cut0} \approx 50\,\mathrm{km\,s^{-1}}$. This difference could arise due to the 1D simulations used by Sobacchi & Mesinger missing 3D substructures that favour a lower value for the critical mass at $z = 0$ (see Section 3.1 in Sobacchi & Mesinger 2013). In what follows, we treat $V_{\rm cut0}$ and α_v as free parameters in the new photoionization feedback model.

In the top left panel of Fig. 3, we show the predicted H I mass function at $z = 0$ for models using $V_{\rm cut}(z)$ (equation 5) with $V_{\rm cut0} = 50\,\mathrm{km\,s^{-1}}$, while varying α_v from -8.2 to -0.2. In the top right panel of Fig. 3, we show the predicted H I mass function for models using $V_{\rm cut}(z)$ and $\alpha_v = -0.8$, while varying $V_{\rm cut0}$ from 35 to 60 $\mathrm{km\,s^{-1}}$ at $z = 0$. The top panels of Fig. 3 show that this model is able to capture the shape of the HIMF down to $M_{\rm H\,I} \sim 10^6\,h^{-2}\,\mathrm{M_\odot}$ much more accurately than the default model does at $z = 0$. This suggests that an evolving photoionization model is preferred by the observations in the local Universe.

We also show the predicted H I mass function at $z = 0.1$ (middle panels) and $z = 0.25$ (bottom panels) in Fig. 3. Interestingly, the predicted H I mass functions at these redshifts show larger variation on changing the parameters of equation (5) than the H I mass function at $z = 0$. Ongoing and future H I-selected galaxy surveys using the Square Kilometre Array (SKA; e.g. Baugh et al. 2004; Power, Baugh & Lacey 2010; Kim et al. 2011) and its pathfinders, such as Australian Square Kilometre Array Pathfinder (ASKAP; cf. Johnston et al. 2008) and Meer Karoo Array Telescope (MeerKAT; cf. Jonas 2007) are expected to extend our view of the H I Universe to higher redshifts. These observations will probe the physical processes that drive galaxy formation, and we expect these surveys to be particularly enlightening regarding how photoionization feedback should be modelled.

Encouraged by the success of this model in the local Universe, we next constrain the parameters of the new photoionization model, $V_{\rm cut0}$ and α_v. For combinations of values $\boldsymbol{\theta} = (V_{\rm cut0}, \alpha_v)$, we obtain the χ^2 of the model with respect to the observed H I mass function, and calculate the likelihood of each combination of parameters,

$$\mathcal{L} \propto \exp\left(-\frac{\chi^2}{2}\right),$$

$$\text{where } \chi^2 = \sum_{i=1}^{N}\frac{[X_i(\boldsymbol{\theta}) - X_{{\rm obs},i}]^2}{\sigma^2_{{\rm obs},i}}, \quad (6)$$

where $X_i(\boldsymbol{\theta})$ and $\sigma_{{\rm obs},i}$ represent the model prediction for the ith observed data point, $X_{{\rm obs},i}$ and its measurement error, respectively. From this two-dimensional likelihood distribution, we estimate the joint 1σ (68.3), 2σ (95.4) and 3σ (99.7 per cent) confidence levels around the best combination of parameters (those that minimize the χ^2). This is shown in Fig. 4 for α_v and $V_{\rm cut0}$.

We find that the combination of parameters, ($V_{\rm cut0}$, α_v) that provides the best fit to the observed H I mass function at $z = 0$ is ($V_{\rm cut0}$, α_v) = (55 $\mathrm{km\,s^{-1}}$, -2.02) for $z_{\rm IN} = 6$ and (50 $\mathrm{km\,s^{-1}}$, -0.82) for $z_{\rm IN} = 10$ (hereafter, our best-fitting model). Two values for $z_{\rm IN}$ are considered to reflect the current uncertainty in the EoR. We find that the best-fitting combination of parameters for $z_{\rm IN} = 6$ are in the 1σ confidence level of the two-dimensional likelihood distribution for the $z_{\rm IN} = 10$ case, indicating that this assumption does not introduce a large uncertainty. These values are shown in the panels (a) and (b) of Fig. 4 by the cross. The likelihoods derived from the modified model correspond to improvements in the predicted low-mass end of the H I mass function, as demonstrated in the panel (c) of Fig. 4, which shows the ratio of the χ^2 value (defined in equation 6) of the default model (that in Lagos et al. 2012) to the value of using the Sobacchi & Mesinger model for $z_{\rm IN} = 10$. Also shown are the three different representative sets of parameters drawn from each confidence level in our modelling, as well as the best-fitting parameter set for $z_{\rm IN} = 10$. The panel (d) of Fig. 4 shows the evolution of $V_{\rm cut}(z)$ for different sets of parameters. The solid black lines show the evolution of $V_{\rm cut}(z)$ from Sobacchi & Mesinger (2013) for two different values of the UV background intensity[2] (1 and 0.01×10^{-21} erg s^{-1} Hz^{-1} cm^{-2} sr^{-1}.) and values for $V_{\rm cut0} \sim$ of 55 and 40 $\mathrm{km\,s^{-1}}$. The blue dashed lines in the right-hand panel of Fig. 4 show the evolution for different combinations of parameters that lie in the 3σ likelihood region, while the red dotted lines show parameter combinations that lie in the 2σ confidence level. The red long dashed line shows the evolution for the best-fitting set of parameters for $z_{\rm IN} = 10$.

We note that in this exercise, α_v and $V_{\rm cut0}$ are varied independently of the other parameters in GALFORM. We have verified that the modified model for photoionization feedback using these parameters does not affect other model predictions that were in good agreement with the observations. This is because these observations tend to probe more massive galaxies than the low-mass end of the H I mass function. For example, Fig. 5 shows the predicted b_J- and K-band luminosity functions in the default model and in the new model, demonstrating that we find broad consistency with observations for galaxies brighter than -15 mag.

4.1 The distribution of H I in central and satellite galaxies

In Fig. 6, we investigate the contributions of satellite and central galaxies to the H I mass function in the default model and in our best-fitting model. The non-monotonic feature seen in the H I mass function from the default model is related to both the suppression of cooling process in central galaxies, and the abundance of

[2] Sobacchi & Mesinger (2013) pointed out that their results are not very sensitive to the intensity of the UVB: increasing the intensity of the UVB by 2 orders of magnitude increases the critical mass only by a factor of 2–3. Measurements of the Lyman alpha forest imply that the UVB intensity lies between (0.1 and 1) $\times 10^{-21}$ erg s^{-1} Hz^{-1} cm^{-2}sr^{-1} at $z = 2$ to 6 (e.g. Bolton & Haehnelt 2007; Haardt & Madau 2012). But its evolution for $z > 6$ is very uncertain.

Downloaded from http://mnras.oxfordjournals.org/ at University of Melbourne on February 15, 2016

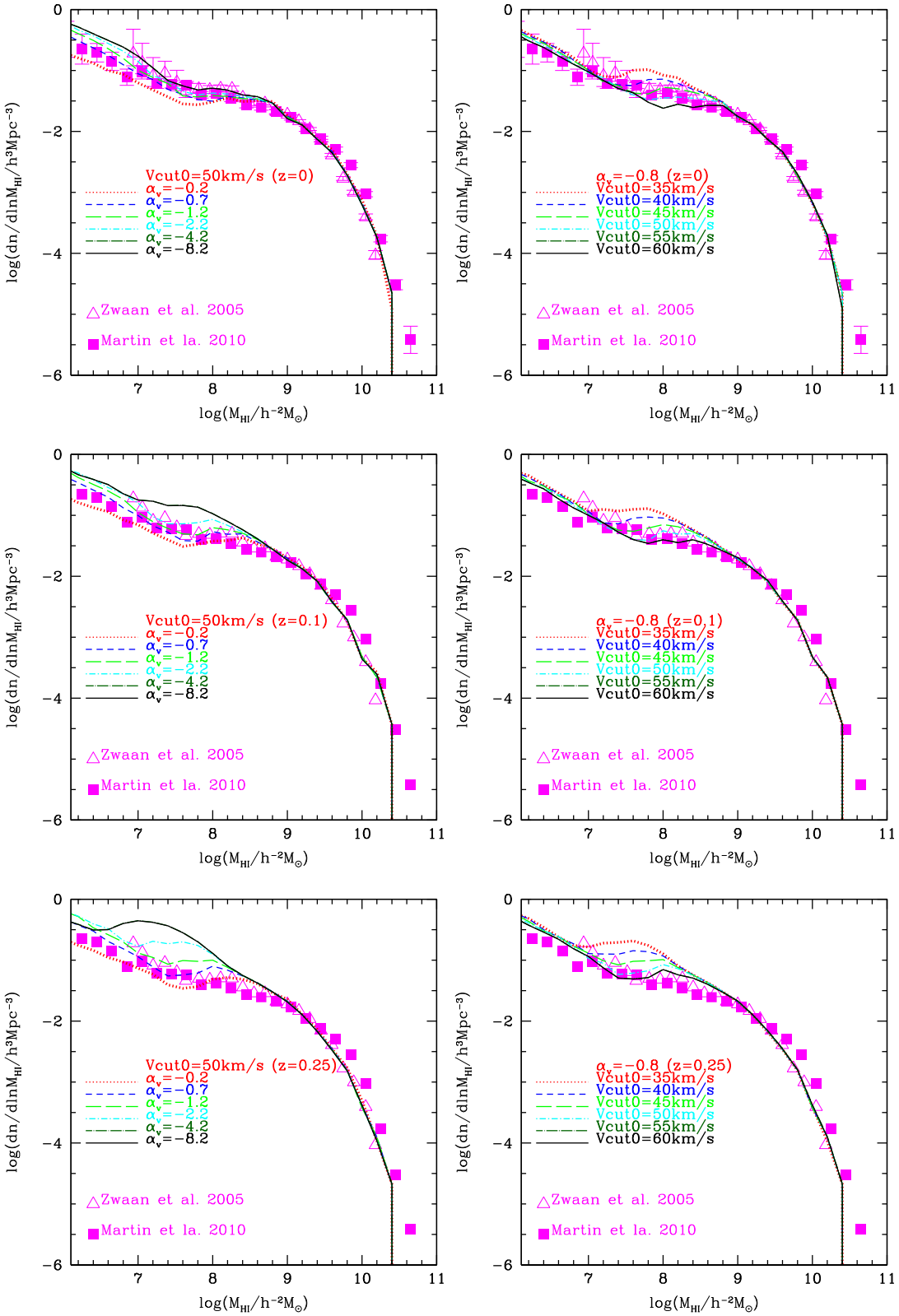


Figure 3. The impact of the redshift-dependent $V_{\rm cut}(z)$ modelling on the predicted H I mass function (top panels) at $z = 0$. The symbols correspond to observations in the local Universe from HIPASS (open triangles; cf. Zwaan et al. 2005) and ALFALFA (filled squares; cf. Martin et al. 2010). Note that these data are reproduced without error bars in the $z = 0.1$ and $z = 0.25$ middle and bottom panels as a reference to illustrate the evolution of the mass function. We vary α_v from -8.2 to -0.2 (which controls the redshift dependence), and $V_{\rm cut0}$ from 35 to 60 km s^{-1}, as labelled. The middle and bottom panels show the predicted H I mass functions at $z = 0.1$ and $z = 0.25$, respectively, for the same combination of parameters shown in the top panels.

Downloaded from http://mnras.oxfordjournals.org/ at University of Melbourne on February 15, 2016

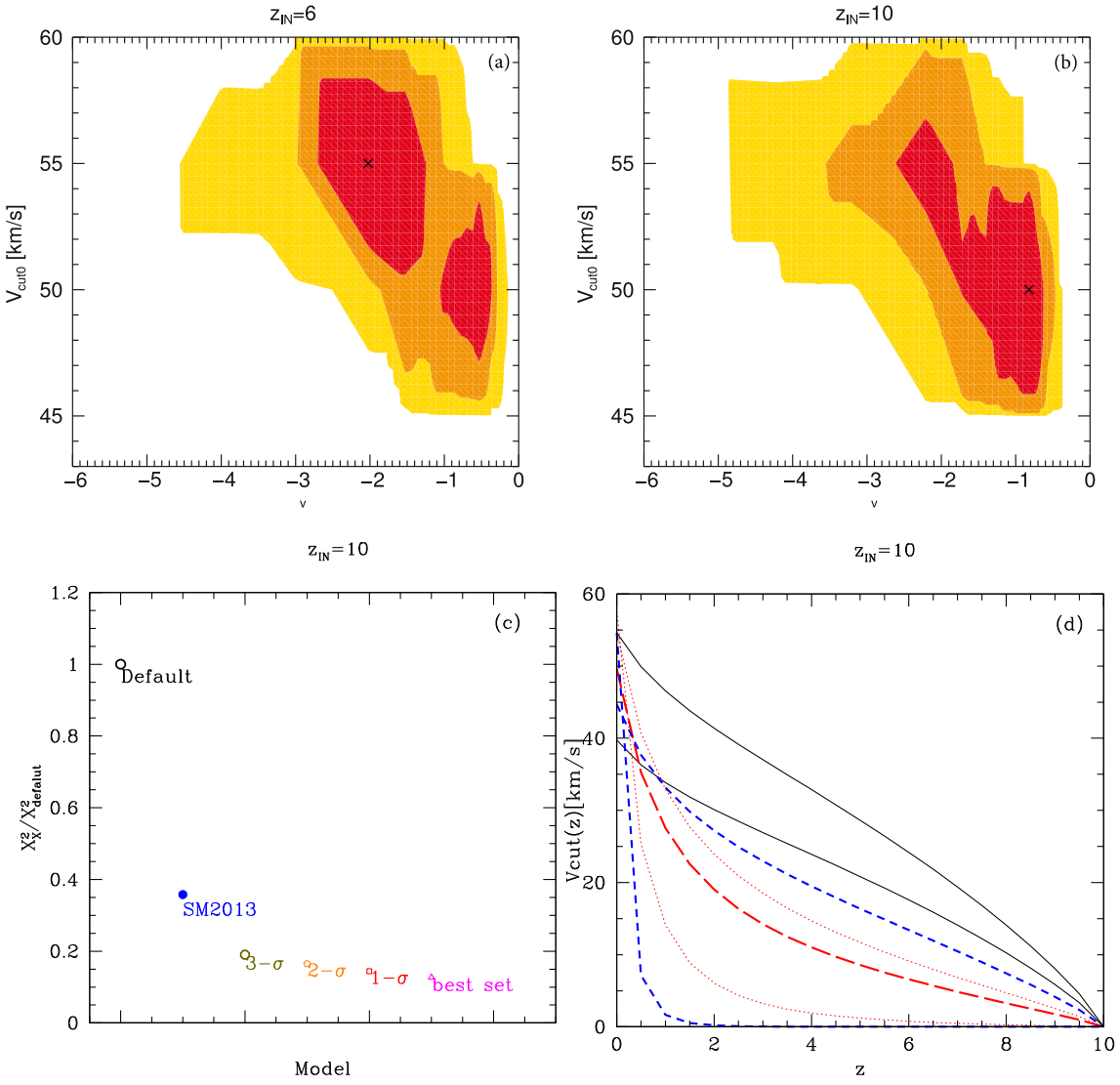


Figure 4. The upper panels (a) and (b) show the likelihood contours and the best-fitting parameters $\alpha_v - V_{\rm cut0}$ (indicated by the cross) for $z_{\rm IN} = 6$ and $z_{\rm IN} = 10$, respectively. The red, orange and yellow colours indicate the 1σ, 2σ and 3σ levels. The maximum likelihood positions are shown as a cross symbols in the figures, $(V_{\rm cut0}, \alpha_v) = (55, -2.02)$ for $z_{\rm IN} = 6$ and $(V_{\rm cut0}, \alpha_v) = (50, -0.82)$ for $z_{\rm IN} = 10$. Sobacchi & Mesinger (2013) suggested $\alpha_v = -0.2$. and $V_{\rm cut0} \sim 55\,(40)\,{\rm km\,s^{-1}}$ (which corresponds to the circular velocity advocated by Sobacchi & Mesigner after reducing their critical halo mass by a factor of 10; see details in Section 4) for UV background intensities of 1 (0.01) [10^{-21} erg s^{-1} Hz^{-1} cm^{-2} sr^{-1}]. The panel (c) shows the ratio of χ^2 (as defined in equation 6) between the default model and the model of Sobacchi & Mesinger (2013, SM2013) adopting a UVB intensity 0.1, parameters using in the three different confidence levels, and the best set of parameters in our modelling for $z_{\rm IN} = 10$. The panel (d) shows the evolution of $V_{\rm cut}(z)$ for ?, solid lines, two different UV background intensity values [0.01,1)sobacchi.etal.2013, two examples from the 2σ likelihood region (dotted red lines), two examples from the 3σ likelihood region (dashed blue lines) and the maximum likelihood position (long dashed red line) for $z_{\rm IN} = 10$.

satellite galaxies at low H I masses. Photoionization feedback in the default model suppresses the cooling of gas in central galaxies which have circular velocities less than $V_{\rm cut}$. As a result, the contribution of central galaxies to the number density of galaxies with $M_{\rm H\,I} \sim 10^6\,h^{-2}\,{\rm M}_\odot$ is less than 10 per cent in the default model. On the other hand, satellite galaxies in massive dark matter haloes ($M_{\rm halo} > 10^{13}\,h^{-1}\,{\rm M}_\odot$) contribute more than 90 per cent of the abundance at galaxy masses of $M_{\rm H\,I} \sim 10^6\,h^{-2}\,{\rm M}_\odot$. Furthermore, in the default model the abundance of satellite galaxies monotonically increases towards low H I mass. The reason why the HIMF of satellite galaxies does not show the dip at low H I masses observed in the HIMF of central galaxies is that the satellites were mainly formed before reionization. Thus, the sum of the abundance of central galaxies and satellite galaxies introduces a non-monotonic feature in the default model around the $M_{\rm H\,I}$ that is directly related to the value of the parameter $V_{\rm cut}$.

The contribution of satellite galaxies to the H I mass function in our best-fitting model is larger than in the default model across the whole H I mass range shown. Central galaxies dominate the abundance of galaxies at $M_{\rm H\,I} \geq 10^8\,h^{-2}\,{\rm M}_\odot$ in both models. However, at $M_{\rm H\,I} \leq 10^7\,h^{-2}\,{\rm M}_\odot$, the abundance of central galaxies drops below the abundance of satellite galaxies in the default model. In contrast, our best-fitting model includes a similar abundance of central and satellite galaxies. The reason is that central galaxies with circular velocities from 30 to 50 km s^{-1} in the default model are never affected by photoionization feedback, while in the new model these are suppressed between $0 \leq z \leq 1$. These central galaxies dominate the H I mass function at $10^6\,h^{-2}\,{\rm M}_\odot \leq M_{\rm H\,I} \leq 10^8 h^{-2}\,{\rm M}_\odot$. In

Downloaded from http://mnras.oxfordjournals.org/ at University of Melbourne on February 15, 2016

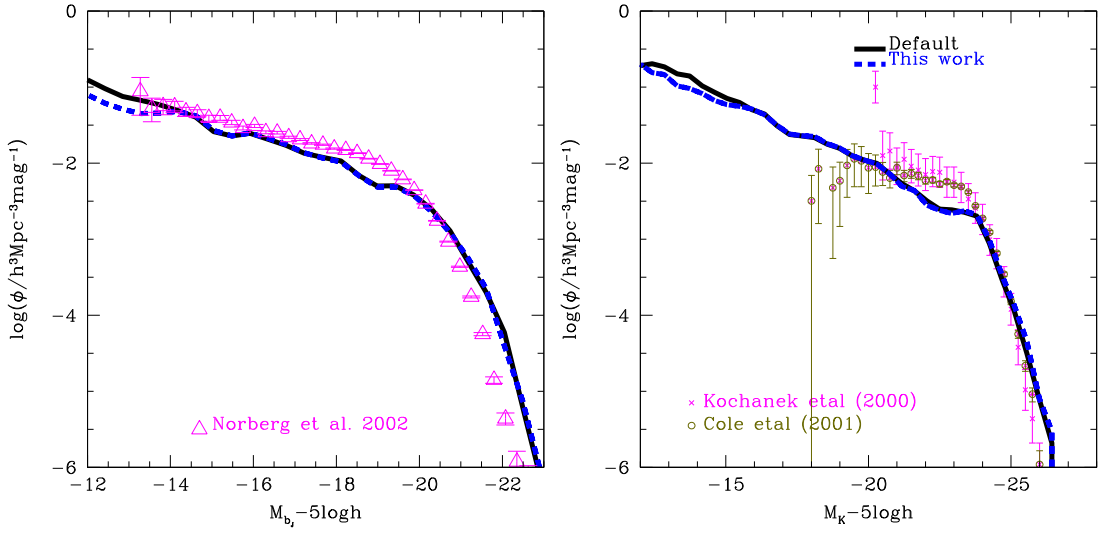


Figure 5. The b_J-band and K-band galaxy luminosity function at $z = 0$ for the default model (black solid line) and our best-fitting model (blue dashed line). Observations from Norberg et al. (2002) for b_J-band luminosity function (left-hand panel) and Cole et al. (2001) and Kochanek et al. (2001) for K-band luminosity functions (right-hand panel) are shown by symbols with error bars.

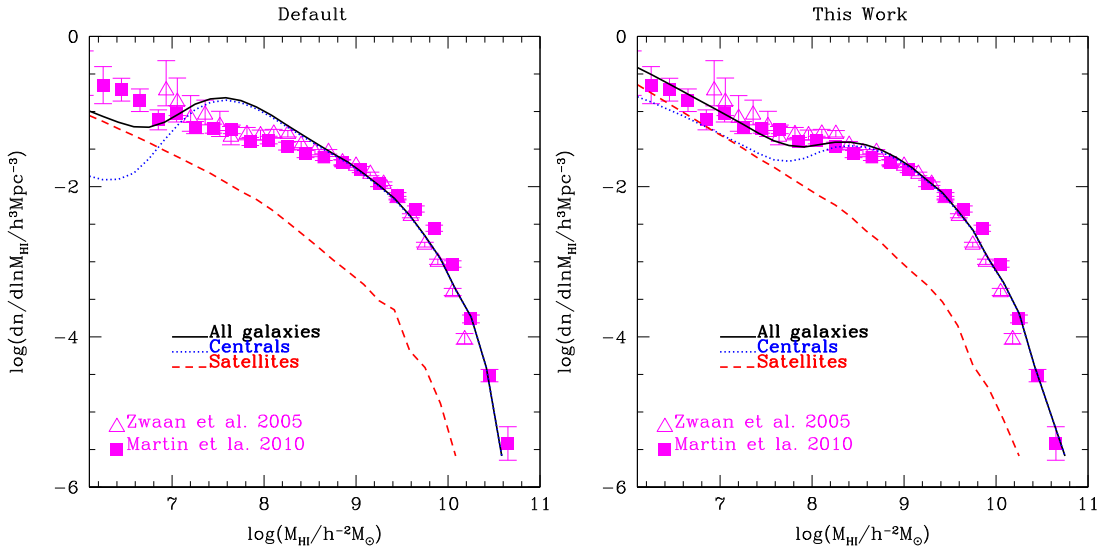


Figure 6. The H I mass functions at $z = 0$ (black solid lines) in the default model (left-hand panel) and the best fit in our new model (right-hand panel). The contributions to the H I mass function, from central galaxies are shown by blue dotted lines and from satellite galaxies as red dashed lines.

addition, central galaxies with circular velocities $\leq$30 km s^{-1} in the default model cannot contain cold gas at $z \leq 10$, and cease forming stars shortly after. In the new model, these galaxies are able to continue accreting new gas and form stars down to $z \sim 1$. This produces the increased abundance of central galaxies at $M_{\rm H\,I} \leq 10^7\,h^{-2}\,{\rm M}_\odot$ that reside in haloes of mass $\leq 10^{10}\,h^{-1}\,{\rm M}_\odot$.

This difference in the abundance of satellite versus central H I galaxies explains why the non-monotonic feature seen in the default model is not found in our new model, providing evidence for an evolution in the strength of photoionization feedback.

5 OTHER PROBES OF PHOTOIONIZATION FEEDBACK

In this section, we examine the effects of the modified model for photoionization feedback on the predicted spatial distribution of galaxies selected by their H I mass, and on the relation between the H I and the stellar mass contents of galaxies at $z = 0$.

5.1 Clustering of H I galaxies

We first use the two-point correlation function to investigate how the modified photoionization feedback influences the spatial distribution of galaxies selected by their H I mass. The distribution of H I-selected galaxies in the default model agrees well with the observations of Meyer et al. (2007) and Martin et al. (2010) who used the HIPASS and the ALFALFA surveys, respectively, to measure the clustering of galaxies with $M_{\rm H\,I} > 10^8\,h^{-2}\,{\rm M}_\odot$ (Kim et al. 2013b). However, it is challenging to measure the spatial distribution of H I-poor galaxies due to the small number of such galaxies observed in current surveys (cf. Papastergis et al. 2013).

The top panel of Fig. 7 shows the predicted two-point correlation functions measured from the default model and for our best-fitting

Downloaded from http://mnras.oxfordjournals.org/ at University of Melbourne on February 15, 2016

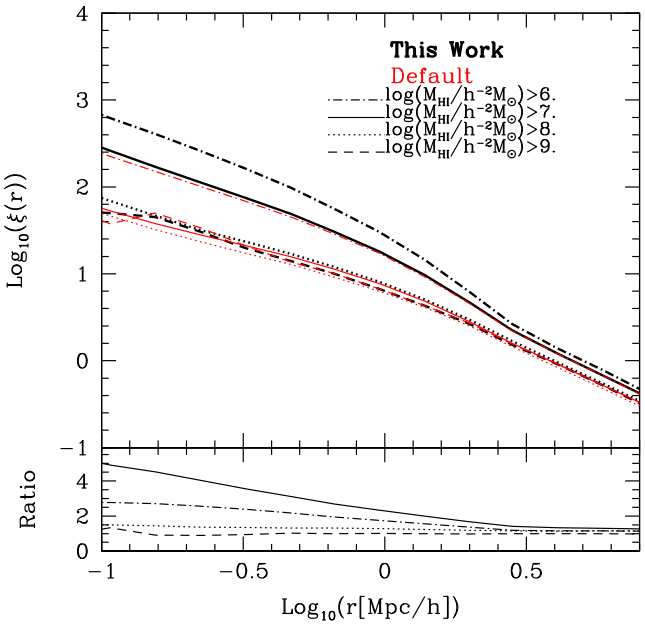


Figure 7. The impact of the modified photoionization feedback model on the two-point correlation function. The lines show the predictions for four galaxy samples defined by different H I mass thresholds (see key). The default model (our best-fitting model) is shown by the thin red (thick black) lines. The lower subpanel shows the ratio of the prediction from the best-fitting model to that from the default model for different H I mass thresholds.

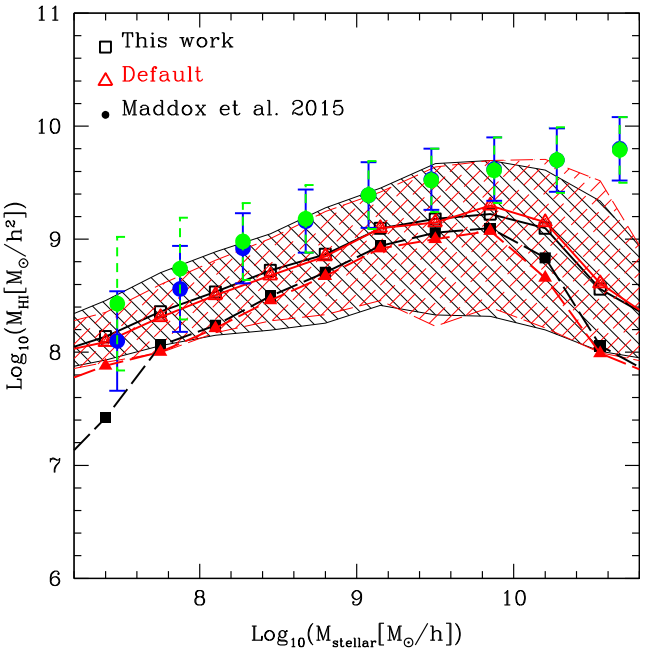


Figure 8. The H I mass as a function of the stellar mass for the default model and our best-fitting model with only galaxies which have H I mass $>10^8\,h^{-2}\,\mathrm{M}_\odot$, stellar mass $>10^7\,h^{-1}\,\mathrm{M}_\odot$ and the bulge-to-total stellar mass ratio < 0.5. The median H I masses in bins of stellar mass are shown for the default model as red empty triangles and our best-fitting model as black empty squares. The shaded regions represent the 16 and 84 per cent range for the default model (red dashed) and our best-fitting model (black solid). The filled circles represent the observations in Maddox et al. (2015). Blue points are derived only from galaxies with SDSS (Sloan Digital Sky Survey) spectra, and green points are derived only from galaxies without spectrum. The error bars correspond to the 1σ dispersion of observation. In comparison, the median H I masses in bins of stellar mass are shown for the default model as red filled triangles and our best-fitting model as black filled squares using lower H I mass threshold ($M_{\mathrm{H\,I}} > 10^6\,h^{-2}\,\mathrm{M}_\odot$).

model, while the bottom panel shows the ratio between the correlation function in the best-fitting model to that in the default model. We consider four H I mass selections in order to see how the modified model for photoionization feedback is imprinted on the clustering of H I-selected galaxies. The predicted two-point correlation functions show that the clustering amplitude in the default model is much lower than in our best-fitting model for the H I mass samples with $M_{\mathrm{H\,I}} > 10^6$ and $M_{\mathrm{H\,I}} > 10^7\,h^{-2}\,\mathrm{M}_\odot$. In addition, the slope of the two-point correlation function at small separations is steeper in our best-fitting model than it is in the default model. The ratios of correlation functions for the H I mass samples with $M_{\mathrm{H\,I}} > 10^6$ and $M_{\mathrm{H\,I}} > 10^7\,h^{-2}\,\mathrm{M}_\odot$ shows a large difference at small separations. This is because the two models have different numbers of satellite galaxies with H I masses in the range 10^6 and $10^8\,h^{-2}\,\mathrm{M}_\odot$, which dominate the small-scale clustering signal.

The increase in the observed number of galaxies with $M_{\mathrm{H\,I}} < 10^7\,h^{-2}\,\mathrm{M}_\odot$ expected from ongoing and future H I galaxy surveys (e.g. ASKAP, MeerKAT, SKA) promises to allow the nature of photoionization feedback to be inferred from the spatial distribution of galaxies with low H I mass.

5.2 Stellar mass–H I mass relation

Fig. 8 shows predictions for the relation between the H I and stellar mass contents of galaxies for both the default model and our best-fit model. These are compared with the observational results for the median H I mass as a function of stellar mass presented by Maddox et al. (2015) (filled circles). Note that we only consider model galaxies which have a H I mass $>10^8\,h^{-2}\,\mathrm{M}_\odot$, a stellar mass $>10^7\,h^{-1}\,\mathrm{M}_\odot$ and a bulge-to-total stellar mass ratio <0.5 in this plot, in order to approximately imitate the selection criteria of the ALFALFA (Maddox, private communication). As argued by Maddox et al. (2015), this relation provides a fundamental benchmark for galaxy formation models by combining H I mass data with stellar mass data. The relation between the H I mass and stellar mass in both models remains in reasonable agreement with the 1σ dispersion of the observations. We note that high stellar mass galaxies in the models typically lie slightly below the observations. This could be due in part to remaining differences between the observational sample selection and the crude cuts applied to the model galaxies to mimic that described above. Indeed, H I observations of stellar mass selected samples show somewhat different behaviour and are in better agreement with the model predictions (Catinella et al. 2010; Serra et al. 2012). Further analysis of the H I gas fraction distribution function of galaxies at $z \sim 0$ from GALFORM and comparison with observations are described in Lagos et al. (2014).

Finally, we note that the model predictions shown in Fig. 8 are the true stellar masses rather than those estimated from photometry or spectra. Mitchell et al. (2013) showed that the process of estimating the stellar mass of a galaxy can lead to differences from the stellar mass predicted directly by the model. These include systematic shifts, which arise from a mismatch between the choice of stellar initial mass function used to estimate the stellar mass and that adopted in the semi-analytic model and from differences in the modelling of dust extinction, and scatter, due to variation in the assumed metallicity and SF history. If we replaced the true model stellar masses in Fig. 8 with estimated stellar masses, this would soften the downturn in the relation at high stellar masses. We also

Downloaded from http://mnras.oxfordjournals.org/ at University of Melbourne on February 15, 2016

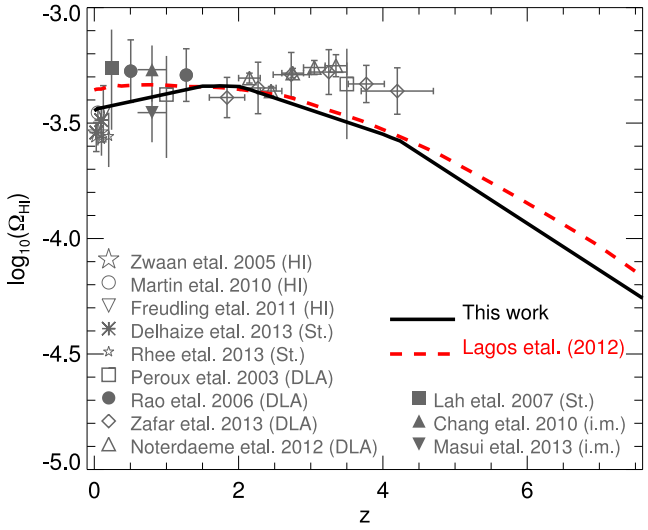


Figure 9. The H I density in units of the critical density as a function of redshift for our $V_{\rm cut}(z)$ model (this work, black solid line) and Lagos et al. (2012) model (red dashed line). The points show various observations. The parenthesis after each observation indicated the method used are H I: direct 21cm line detection (Zwaan et al. 2005; Martin et al. 2010; Freudling et al. 2011), St.: stacking of 21cm line (Lah et al. 2007; Delhaize et al. 2013; Rhee et al. 2013), DLA: absorption line studies (Péroux et al. 2003; Rao, Turnshek & Nestor 2006; Noterdaeme et al. 2012; Zafar et al. 2013) and i.m.: intensity mapping of the 21cm line (Chang et al. 2010; Masui et al. 2013).

include the predictions from the two models using a lower H I mass threshold ($M_{\rm H\,I} > 10^6\,h^{-2}\,{\rm M}_\odot$ instead of $M_{\rm H\,I} > 10^8\,h^{-2}\,{\rm M}_\odot$; see red filled triangles for the default model and the black filled squares for our best-fitting new model connected by long dashed lines for the median H I masses in bins of stellar mass). The predictions deviate from one another at stellar masses between 10^7 and $10^8\,h^{-1}\,{\rm M}_\odot$. This stellar mass range corresponds to H I masses between 10^6 and $10^8\,h^{-2}\,{\rm M}_\odot$, where the two models also predict different H I abundances because of the different modelling of photoionization feedback.

5.3 Evolution of H I density

Finally, we investigate the impact of our new model on the H I density as a function of redshift. Fig. 9 shows $\Omega_{\rm H\,I}$, defined as the ratio between the mean H I density and the critical density of the Universe, for the new evolving $V_{\rm cut}(z)$ model (black solid line) and the Lagos et al. (2012) model (red dashed line, the default model). The H I density predicted using the new model with $V_{\rm cut}(z)$ shows slightly better agreement with the observed H I density at $z < 0.1$ than the Lagos et al. (2012) model, recovering the decreases $\Omega_{\rm H\,I}$ suggested by the observations of $z \geq 0.2$. However, the difference between the two models are within the uncertainties of the observations, and new constraints at intermediate redshifts are needed.

6 SUMMARY

One of the most important ingredients in a model of galaxy formation is the description of neutral hydrogen which provides the fuel for SF. The HIPASS Zwaan et al. (2005) and ALFALFA Martin et al. (2010) surveys have been used to estimate the H I mass function down to masses of a few times $10^6\,h^{-2}\,{\rm M}_\odot$ in the local Universe. Attempting to reproduce these observed H I mass functions using a galaxy formation model allows us to probe the physics of low-mass galaxy formation.

In the standard implementation of GALFORM, the effect of photoionization feedback is modelled by restricting galaxy formation in haloes which correspond to effective circular velocities smaller that a fixed circular velocity of $V_{\rm cut}$ at redshifts following the end of reionization $z_{\rm cut}$ (the default model). Haloes with circular velocities below $V_{\rm cut}$ are not allowed to cool gas at redshifts below $z_{\rm cut}$. The predicted H I mass function from this default model shows good agreement with observations of the H I mass function for masses greater than $M_{\rm H\,I} \sim 10^8\,h^{-2}\,{\rm M}_\odot$. However, the default model fails to explain the abundance of galaxies with H I masses between 10^6 and $10^8\,h^{-2}\,{\rm M}_\odot$.

There are several possibilities to ease the discrepancy at the low-mass end of the H I mass function between observations and the default model, including changing the SN feedback, cosmological parameters and the form of the SF law in the model. In particular, Kim et al. (2013a) showed that photoionization feedback is an important physical processes for the low-mass end of H I mass function. We have investigated these possibilities using a version of the GALFORM semi-analytical galaxy formation model (cf. Cole et al. 2000) by Lagos et al. (2012) to simulate the low-mass end of the H I mass function. In our investigation, we showed that varying the SNe feedback, the efficiency of SF and the cosmological model all failed to explain the shape and abundance of the low-mass end of H I mass function. Varying the redshift and critical velocity of galaxy suppression of formation by photoionization feedback from reionization is also unable to explain the shape of the low-mass end of H I mass function.

To understand what photoionization physics affects the shape and abundance of the H I mass function in the local Universe, we introduced a redshift-dependent photoionization feedback into GALFORM, motivated by the simulations of Sobacchi & Mesinger (2013). This illustrates the modular nature of semi-analytical modelling, whereby the treatment of a given physical process can be overhauled and improved when new information becomes available. We find that redshift-dependent modelling of feedback from photoionization on low-mass galaxy formation is needed to explain the shape and abundance of the observed H I mass function in the local Universe. We also find that the sensitivity of the H I mass function to the redshift evolution of photoionization feedback strength is larger at high redshift. Our modelling suggests that future measurements of H I clustering in low-mass galaxies and the relation between the H I mass and the stellar mass of galaxies will provide additional constraints on the form of ionizing feedback.

Ongoing and future H I-selected galaxy surveys on the SKA and its pathfinders, such as ASKAP, MeerKAT are expected to extend our view of the H I Universe to higher redshifts not only for the H I mass function but also for the distribution of H I galaxies. The evolution of the H I mass function as a function of redshift will tell us about the physical processes that drive low-mass galaxy formation, including photoionization feedback.

ACKNOWLEDGEMENTS

H-SK is supported by a Discovery Early Career Researcher Awards from the Australian Research Council (DE140100940). CP thanks Simon Driver and Aaron Robotham for helpful discussions. CP is supported by DP130100117, DP140100198 and FT130100041. CL is funded by the ARC project DE150100618. This work was supported by a STFC rolling grant at Durham. The calculations for this paper were performed on the ICC Cosmology

Downloaded from http://mnras.oxfordjournals.org/ at University of Melbourne on February 15, 2016

Machine, which is part of the DiRAC Facility jointly funded by the STFC, the Large Facilities Capital Fund of BIS, and Durham University. Part of the research presented in this paper was undertaken as part of the Survey Simulation Pipeline (SSimPL; http://www.astronomy.swin.edu.au/SSimPL/). The Centre for All-Sky Astrophysics is an Australian Research Council Centre of Excellence, funded by grant CE110001020.

REFERENCES

Barkana R., Loeb A., 2007, Rep. Prog. Phys., 70, 627
Baugh C. M., 2006, Rep. Prog. Phys., 69, 3101
Baugh C. M., Lacey C. G., Frenk C. S., Benson A. J., Cole S., Granato G. L., Silva L., Bressan A., 2004, New Astron. Rev., 48, 1239
Benson A. J., Lacey C. G., Baugh C. M., Cole S., Frenk C. S., 2002, MNRAS, 333, 156
Bigiel F., Leroy A., Walter F., Blitz L., Brinks E., de Blok W. J. G., Madore B., 2010, AJ, 140, 1194
Blitz L., Rosolowsky E., 2006, ApJ, 650, 933
Bolton J. S., Haehnelt M. G., 2007, MNRAS, 374, 493
Bower R. G., Benson A. J., Malbon R., Helly J. C., Frenk C. S., Baugh C. M., Cole S., Lacey C. G., 2006, MNRAS, 370, 645
Brown T. M. et al., 2014, ApJ, 796, 91
Catinella B. et al., 2010, MNRAS, 403, 683
Chang T., Pen U., Bandura K., Peterson J. B., 2010, Nature, 466, 463
Cole S., Aragon-Salamanca A., Frenk C. S., Navarro J. F., Zepf S. E., 1994, MNRAS, 271, 781
Cole S., Lacey C. G., Baugh C. M., Frenk C. S., 2000, MNRAS, 319, 168
Cole S. et al., 2001, MNRAS, 326, 255
Delhaize J., Meyer M. J., Staveley-Smith L., Boyle B. J., 2013, MNRAS, 433, 1398
Dijkstra M., Haiman Z., Rees M. J., Weinberg D. H., 2004, ApJ, 601, 666
Efstathiou G., 1992, MNRAS, 256, 43P
Elmegreen B. G., 1993, ApJ, 411, 170
Font A. S. et al., 2011, MNRAS, 417, 1260
Freudling W. et al., 2011, ApJ, 727, 40
Giovanelli R. et al., 2005, AJ, 130, 2598
Gnedin N. Y., 2000, ApJ, 535, 530
Gonzalez-Perez V., Lacey C. G., Baugh C. M., Lagos C. D. P., Helly J., Campbell D. J. R., Mitchell P. D., 2014, MNRAS, 439, 264
Haardt F., Madau P., 2012, ApJ, 746, 125
Hoeft M., Yepes G., Gottlöber S., Springel V., 2006, MNRAS, 371, 401
Johnston S. et al., 2008, Exp. Astron., 22, 151
Jonas J., 2007, in From Planets to Dark Energy: the Modern Radio Universe MeerKAT Science and Technology, Univ. Manchester, UK p. 7
Kim H.-S., Baugh C. M., Benson A. J., Cole S., Frenk C. S., Lacey C. G., Power C., Schneider M., 2011, MNRAS, 414, 2367
Kim H.-S., Power C., Baugh C. M., Wyithe J. S. B., Lacey C. G., Lagos C. D. P., Frenk C. S., 2013a, MNRAS, 428, 3366
Kim H.-S., Wyithe J. S. B., Park J., Lacey C. G., 2013b, MNRAS, 433, 2476
Kochanek C. S. et al., 2001, ApJ, 560, 566
Krumholz M. R., McKee C. F., Tumlinson J., 2009, ApJ, 699, 850
Lagos C. D. P., Lacey C. G., Baugh C. M., Bower R. G., Benson A. J., 2011a, MNRAS, 416, 1566
Lagos C. D. P., Baugh C. M., Lacey C. G., Benson A. J., Kim H.-S., Power C., 2011b, MNRAS, 418, 1649
Lagos C. d. P., Bayet E., Baugh C. M., Lacey C. G., Bell T. A., Fanidakis N., Geach J. E., 2012, MNRAS, 426, 2142
Lagos C. d. P., Lacey C. G., Baugh C. M., 2013, MNRAS, 436, 1787
Lagos C. d. P., Davis T. A., Lacey C. G., Zwaan M. A., Baugh C. M., Gonzalez-Perez V., Padilla N. D., 2014, MNRAS, 443, 1002
Lah P. et al., 2007, MNRAS, 376, 1357
Leroy A. K., Walter F., Brinks E., Bigiel F., de Blok W. J. G., Madore B., Thornley M. D., 2008, AJ, 136, 2782
McGreer I. D., Mesinger A., Fan X., 2011, MNRAS, 415, 3237
Maddox N., Hess K. M., Obreschkow D., Jarvis M. J., Blyth S.-L., 2015, MNRAS, 447, 1610
Martin A. M., Papastergis E., Giovanelli R., Haynes M. P., Springob C. M., Stierwalt S., 2010, ApJ, 723, 1359
Masui K. W. et al., 2013, ApJ, 763, L20
Mesinger A., Furlanetto S., Cen R., 2011, MNRAS, 411, 955
Meyer M. J. et al., 2004, MNRAS, 350, 1195
Meyer M. J., Zwaan M. A., Webster R. L., Brown M. J. I., Staveley-Smith L., 2007, ApJ, 654, 702
Mitchell P. D., Lacey C. G., Baugh C. M., Cole S., 2013, MNRAS, 435, 87
Norberg P. et al., 2002, MNRAS, 336, 907
Noterdaeme P. et al., 2012, A&A, 547, L1
Okamoto T., Gao L., Theuns T., 2008, MNRAS, 390, 920
Ouchi M. et al., 2010, ApJ, 723, 869
Papastergis E., Giovanelli R., Haynes M. P., Rodríguez-Puebla A., Jones M. G., 2013, ApJ, 776, 43
Parkinson H., Cole S., Helly J., 2008, MNRAS, 383, 557
Péroux C., McMahon R. G., Storrie-Lombardi L. J., Irwin M. J., 2003, MNRAS, 346, 1103
Power C., Baugh C. M., Lacey C. G., 2010, MNRAS, 406, 43
Rao S. M., Turnshek D. A., Nestor D. B., 2006, ApJ, 636, 610
Rees M. J., 1986, MNRAS, 218, 25P
Rhee J., Zwaan M. A., Briggs F. H., Chengalur J. N., Lah P., Oosterloo T., van der Hulst T., 2013, MNRAS, 435, 2693
Robertson B. E., Ellis R. S., Dunlop J. S., McLure R. J., Stark D. P., 2010, Nature, 468, 49
Serra P. et al., 2012, MNRAS, 422, 1835
Shapiro P. R., Iliev I. T., Raga A. C., 2004, MNRAS, 348, 753
Shull J. M., Harness A., Trenti M., Smith B. D., 2012, ApJ, 747, 100
Sobacchi E., Mesinger A., 2013, MNRAS, 432, L51 (SM2013)
Springel V. et al., 2005, Nature, 435, 629
Thoul A. A., Weinberg D. H., 1996, ApJ, 465, 608
Zafar T., Peroux C., Popping A., Milliard B., Deharveng J.-M., Frank S., 2013, A&A, 556, 141
Zwaan M. A., Meyer M. J., Staveley-Smith L., Webster R. L., 2005, MNRAS, 359, L30

This paper has been typeset from a TEX/LATEX file prepared by the author.

Downloaded from http://mnras.oxfordjournals.org/ at University of Melbourne on February 15, 2016